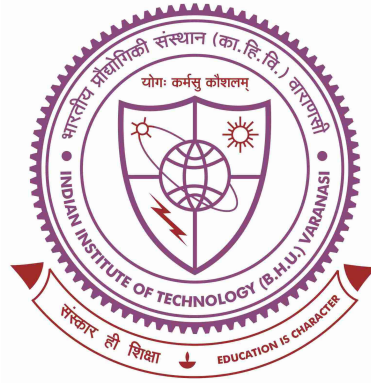


**EVOLUTION OF TRIAXIAL SHAPE IN  $A \sim 120$ : THE  
CASE OF  $^{125}\text{Xe}$ ,  $^{114}\text{Te}$ , AND  $^{119}\text{I}$**



**Thesis submitted in partial fulfillment  
for the Award of  
DOCTOR OF PHILOSOPHY  
in  
PHYSICS**

*by*  
**MAMTA PRAJAPATI**

**DEPARTMENT OF PHYSICS  
INDIAN INSTITUTE OF TECHNOLOGY  
BANARAS HINDU UNIVERSITY  
VARANASI - 221005**

**ROLL NUMBER  
19171505**

**YEAR OF SUBMISSION  
2025**

I would like to dedicate this thesis to my loving parents, brother, sister, and amazing friends, who have encouraged me through this journey.

## Certificate

It is certified that the work contained in the thesis titled “**Evolution of triaxial shape in A ~ 120 : The case of  $^{125}\text{Xe}$ ,  $^{114}\text{Te}$ , and  $^{119}\text{I}$** ” by Ms. Mamta Prajapati, Roll Number **19171505**, has been carried out under my supervision and this work has not been submitted elsewhere for a degree.

**Signature:**



**Supervisor**

Dr. Somnath Nag

(Assistant Professor)

Department of Physics

Indian Institute of Technology (BHU),

Varanasi-221005 (U.P.), India

## Declaration

I, **Mamta Prajapati**, declare that the work included in this thesis is my own bona-fide work and carried out by me under the supervision of **Dr. Somnath Nag** from January 2020 to April 2025 at the **Department of Physics**, Indian Institute of Technology (BHU), Varanasi. The matter embodied in this thesis has not been submitted for the award of any other degree or diploma. I certify that I have faithfully acknowledged and given credits to the research workers whenever and wherever their works have been cited in my work in this thesis. I further declare that I have not wilfully copied any others' work, paragraphs, text, data, results, etc., reported in journals, books, magazines, reports, dissertations, theses, etc., or available at websites and have not included them in this thesis and have not cited as my own work.

Date: 8.4.2025

Place: IIT (BHU), Varanasi

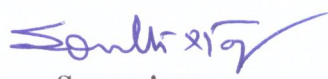
Mamta  
Prajapati

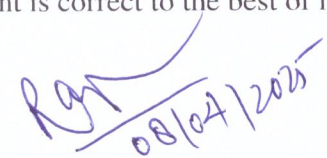
Signature of the Student

(Mamta Prajapati)

## Certificate by the Supervisor

It is certified that the above statement made by the student is correct to the best of my knowledge.

Signature:   
Supervisor  
(Dr. Somnath Nag)

  
Signature of the Head of the Department  
(Prof. Rajendra Prasad)

## Copyright Transfer Certificate

**Title of the Thesis :** Evolution of triaxial shape in  $A \sim 120$  : The case of  $^{125}\text{Xe}$ ,  $^{114}\text{Te}$ , and  $^{119}\text{I}$

**Name of the Student :** Mamta Prajapati

### Copyright Transfer

The undersigned hereby assigns to the Indian Institute of Technology (Banaras Hindu University) Varanasi all rights under copyright that may exist in and for the above thesis submitted for the award of the **Doctor of Philosophy in Physics**.

Date: 8. 1. 2025

*Mamta Prajapati*  
Signature of the Student

Place: IIT (BHU), Varanasi

(Mamta Prajapati)

**Note: However, the author may reproduce or authorize others to reproduce material extracted verbatim from the thesis or derivative of the thesis for author's personal use provided that the source and the Institute's copyright notice are indicated.**

## Acknowledgements

As I reflect on the journey that has led me to the completion of this PhD, I am reminded of the many twists and turns that have shaped not only my academic growth but my life as a whole. This journey has been long, challenging, and filled with moments of doubt, yet also full of learning. I am forever grateful to those who have helped me along this journey.

I am deeply grateful to my supervisor, **Dr. Somnath Nag**, whose unwavering patience, invaluable academic and personal support have been a constant source of support throughout my thesis work; without their dedicated supervision, it would have been impossible to complete this thesis. From the beginning, he created an environment where I felt encouraged to explore ideas, ask questions, and develop my research with confidence. His ability to remain calm and composed even in moments of difficult situations has been an inspiration to me. I feel truly fortunate to have the privilege of working under their mentorship.

I would like to extend my heartfelt thanks to **Prof. Ajay Kumar Singh (IIT Kharagpur)** for their exceptional mentorship, support, and thoughtful discussions throughout my research. Our many conversations focused on specific aspects of my research topics have consistently provided me with new insights and ideas, which have been pivotal to the development of this thesis. I would like to express my gratitude to **Dr. Haridas Pai, Dr. Subhendu Rajabanshi** and **Dr. Saikat Chakraborty** for their suggestions and enthusiastic discussion with them, which helped me to find my firm grounding in the research problem. It has been an honor to collaborate with them, and I truly value the learning and growth that resulted from their collaboration.

I am thankful to **Prof. R. Palit** for providing an experimental slot at TIFR, Mumbai. His insightful assistance in analyzing the results helped me to add an extra chapter to my thesis with a new experiment. I also want to appreciate the support obtained from **Dr.**

**Sarmishtha Bhattacharyya and Dr. Gopal Mukherjee.** They allowed me to actively participate in the VECC-INGA setup, which was a fantastic experience.

I also want to convey my sincere appreciation to **Dr. Deepika Choudhury.** I enjoy meeting and talking to her. She always motivated me regarding my career. Whether it is an academic discussion or a personal one, she gives me a lot of inspiration. I would also like to thank **Prof. Tarkeshwar Trivedi, P. C. Srivastava, J. Meng, and F. F. Xu** for their suggestions and support.

I would like to express my sincere gratitude to **H. Hübel and R. V. F. Janssens** for their invaluable contributions to my first paper. Their insights, expertise, and tireless effort in reviewing and refining the content were incredible. I also want to extend my sincere thanks to A. Al-Khatib, H. Hübel, A. Neußer-Neffgen, G. B. Hagemann, G. Sletten, B. Herskind, C. R. Hansen, G. Benzoni, A. Bracco M. P. Carpenter and P. Chowdhury for their help during the time of the experiment.

I am thankful to the RPEC members, Dr. Gauhar Abbas and Dr. Debdas Ghosh, for their constructive suggestions during this journey. I would stay grateful to the Department of Physics at IIT (BHU). I am grateful to the department's HODs, Prof. Rajendra Prasad and Prof. S. Chatterjee. Furthermore, I would remain indebted to the department's faculty members. The institute's non-teaching personnel deserve special recognition for their contributions to the smooth execution of all needed administrative tasks.

A sincere appreciation is given for the financial help obtained from the Department of Science and Technology during this period. The funding to my supervisor from SERB-DST (ANRF) under contract no. CRG/2021/006671 is also acknowledged.

All through the PhD work, I enjoyed the company of my labmates, **Nidhi Goel and Aalakh Kumar.** We have completed many journeys together regarding experiments and conferences. I have shared very special moments with Nidhi Di. During the COVID time, starting research was really difficult for me and Nidhi Di, We used to relax by discussing

our concerns with each other. I have also shared some joyful moments with my junior Aalakh Kumar, whose playful nature and sense of humor provided much-needed moments of lightheartedness during the stressful phases of my PhD. His ability to make us laugh even in the toughest times reminded me of the importance of balancing hard work with fun. Beyond being a junior, he supported me like a friend in every challenging moment. I'd like to thank you both for being such a consistent source of joy and encouragement.

I would like to thank my wonderful friends **Vartika Singh and Swayangsiddha Ghosh** for their constant support and encouragement throughout my PhD journey. Your friendship, understanding, and words of encouragement helped me get through the toughest times. I'm truly grateful for each of you. Additionally, their motivation to maintain a regular gym routine boosted my physical health. I hope to always be there for you in the same way you have been for me. Thank you for being a positive force in my life. A heartfelt thanks to my junior Abhishek Maurya for his help in arranging this thesis.

I shared fruitful moments with TIFR and VECC group members during the time of experiments. I would like to thank Vishal Malik, Piku Dey, Dr. Ananya Kundu, Dr. Biswajit Das, and also the scientific officers Abraham T Vazhappilly, S. Jadhav, and B. S. Naidu of the TIFR institute for their help. I'd also like to thank Shefali Di, Anandgopal, Satya Samiran Nayak, Snigdha Pal, Suchorita, Soumik Da, and Imran Da for their compassionate treatment throughout my stay at VECC.

I would also like to thank my seniors, Dr. Sutanu Bhattacharya, Dr. Arunita Mukharjee, Atryee Dey, and Dr. Sajad Ali. Sutanu da has always helped me a lot. I always get a positive vibe after talking to him. I have also shared joyful moments with my colleagues and juniors from another institute. I want to mention their names also: Sahab Singh, Rajat Roy, Shreya Tiwari, Rupesh Kumar, Gourchand Manna, Sagar Roy, and Habibur Rahaman.

This long journey of PhD can never be completed without the unwavering love, support, and patience of my family. I am deeply indebted and grateful to my parents, brother, sister,

and the rest of my family members. Their encouragement during the toughest times has been my guiding light. I would like to give a special thanks to my brother, who aroused my curiosity about studies. He has supported me a lot. Finally, my niece and nephews Shivank, Shivam, Aditi, Titu, Pari, Piku, Khushi, Abhijeet, and Anishka also deserve special thanks. Their laughter and playful antics brought joy to even the most challenging days, reminding me of the importance of family and the simple pleasures in life. I am truly grateful for the moments we shared, as they have created lasting memories that I will cherish forever.

The atmosphere of this beautiful green campus not only beautifies the area but also promotes a healthy, conducive space for learning and collaboration. And lastly, I want to thank the grace and kindness of god for everything.

I sincerely apologize for the unintentional exclusion of any name from the above list of acknowledgments. —

**Mamta Prajapati**

---

## List of Acronyms

---

Acronym	Full form
ADC	Analog to Digital Converter
ACQ	Acquisition
BGO	Bismuth Germanate
CFD	Constant Fraction Discriminator
CNS	Cranked Nilsson Strutinsky
CU	Coincidence Unit
DCO	Directional Correlation
DDAQ	Digital Data Acquisition
FADC	Flash Analog to Digital Converter
FET	Field Effect Transistor
FIFO	Fast-In Fast-Out
FWHM	Full Width at Half Maximum
HPGe	High-Purity Germanium
INGA	Indian National Gamma Array
IPDCO	Integrated Polarization-Directional Correlation
LD	Liquid Drop
LDM	Liquid Drop Model
LSD	Lublin-Strasbourg Drop
LVDS	Low Voltage Differential Signalling
MARCOS	Multi Parameter Time-Stamp-Based Coincidence Search Program
PDCO	Polarization-Directional Correlation
PES	Potential Energy Surface
PT	Peak to Total
RLD	Rotating Liquid Drop
TFA	Timing Filtering Amplifier
TIFR	Tata Institute of Fundamental Research

---

---

## List of Symbols

---

Symbols	Definition (unit)
$A$	Mass number
$\alpha$	Signature quantum number
$\beta$	Axial deformation parameter
$\Delta$	Pairing gap energy
$\Delta_{asym}$	Polarization asymmetry parameter
$\epsilon_2$	Quadrupole deformation parameter
$e_i$	Single-particle energy in MeV
$E$	Energy in proper units
$E2$	Electric quadrupole transition
$\gamma$	Triaxiality deformation parameter
$\hbar$	Reduced Plank constant ( $m^2kg/s$ )
$\mathcal{H}$	Hamiltonian
$I$	Total angular momentum of the nucleus
$i_x$	Aligned angular momentum in units of $\hbar$
$j$	Total angular momentum of nucleons; $j = l + s$
$j_x$	Projection of total angular momentum of on x axis
$J$	Moment of inertia of the system
$J_{rig}$	Rigid body moment of inertia
$J^{(1)}$	Kinematic moment of inertia of the system ( $\hbar/MeV$ )
$J^{(2)}$	Dynamic moment of inertia of the system ( $\hbar^2/MeV$ )
$l$	Orbital angular momentum
$\lambda$	Multipole mode
$\Lambda$	Projection of orbital quantum number along the symmetry axis
$m/M$	Mass
$\mu$	Reduced mass
$m_o$	Rest mass of the electron
$M1$	Magnetic dipole transition

---

---

<b>Symbols</b>	<b>Definition (unit)</b>
$N$	Neutron number
$N_q$	Principal quantum number
$\omega$	angular frequency
$\Omega$	The projection of angular momentum along the symmetry axis
$R$	Radius in appropriate units
$R_\theta$	Angular distribution ratio
$s$	Spin angular momentum
$\Sigma$	Projection of spin quantum number along the symmetry axis
$\theta$	Angle
$V$	Potential in appropriate units
$Y_{20}(\theta, \phi)$	Spherical polar harmonics
$Z$	Proton number

---



# List of Figures

1.1	Schematic diagram of the shape parameters in rotating quadrupole-deformed nuclei. . . . .	3
1.2	Pictorial representation of triaxial shape with three unequal axes. . . . .	4
1.3	Calculated reduction in the nuclear ground-state energy when axial symmetry is broken, relative to calculations limited to axially symmetric shapes only. . . . .	5
1.4	Calculated energy levels of a $\gamma$ band using Davydov model. . . . .	7
1.5	Geometrical representation of chiral configuration in a nucleus. . . . .	9
1.6	Geometrical representation of simple wobblers in even-even nucleus. . . .	11
1.7	The moments of inertia of the three principal axes as a function of the triaxiality parameter $\gamma$ . The term "hydro" denotes the irrotational flow values and "cranking" the cranking values, which are scaled by the factor $\mathcal{I}_m^{hyd}(\gamma)/\mathcal{I}_m^{crank}(\gamma)$ . . . . .	12
1.8	Pictorial representation of longitudinal and transverse wobbling motion in odd-A nucleus. . . . .	13
1.9	Pictorial representation of the difference in center of mass and center of charge distribution. . . . .	14
1.10	Potential energy surface plot with respect to $\beta_3$ for octupole vibration and octupole deformed shape. . . . .	15

---

2.1	Schematic diagram illustrating the various modes of formation and decay of a compound nucleus. . . . .	20
2.2	Excitation energy as a function of spin for the decay of the compound nucleus in a heavy-ion-induced fusion-evaporation reaction. The Figure is taken from Ref. 71 . . . . .	21
2.3	The energy dependence of the various $\gamma$ -ray interaction processes. . . . .	23
2.4	Schematic diagram of an escape-suppressed HPGe detector as used in the Gammasphere array. . . . .	26
2.5	Schematic diagram of clover detector. . . . .	28
2.6	Schematic diagram of a view of the Gammasphere spectrometer. Figure taken from Ref. 76 . . . . .	31
2.7	Schematic representation of segmented Ge detectors. Figure taken from Ref. 76 . . . . .	31
2.8	INGA set up at T.I.F.R. Mumbai (left panel) and VECC Kolkata (right panel). . . . .	32
2.9	Schematic representation of the experimental set-up of Gammasphere array. Figure taken from Ref. 78 . . . . .	35
2.10	Block diagram of Pixie-16 module. Figure taken from Ref. 83 . . . . .	36
2.11	The effect of both energy calibration and gain matching is shown for all the crystals of a clover detector. . . . .	38
2.12	Relative efficiency vs energy plot for all the detectors of INGA set up at TIFR. . . . .	41
2.13	A representative partial level-scheme showing coincidence relation. . . . .	42
2.14	The angular distribution of pure dipole (black solid line), pure quadrupole (red solid line), and mixed (blue and olive solid lines) $\gamma$ -ray transitions. . . . .	44

- 2.15 Figure shows the angles in a directional correlation of two  $\gamma$  transitions emitted from an oriented nucleus.  $\phi$  is the angle between the two planes opened by each detector and the beam axis. . . . . 46
- 2.16 Figure shows the comparison between the experimental and calculated values of  $R_{DCO}$  at different value of  $(\sigma/j)$ . . . . . 48
- 2.17 Figure shows the use of a clover detector as a Compton polarimeter. The explanations of the relevant angles ( $\theta, \varepsilon, \phi$ , and  $\zeta$ ), shown in the above figure, are given in the text. . . . . 49
- 2.18 Figure shows the asymmetry correction factor at different energies of  $\gamma$  transitions. . . . . 53
- 3.1 Angular momentum generation via collective rotation in deformed  $^{158}\text{Er}$  nucleus and through single-particle excitation in nearly-spherical nucleus  $^{146}\text{Gd}$ . . . . . 56
- 3.2 Alignment of the particle-hole angular momentum in case of oblate (a) and prolate (b) shapes.  $\Omega$  represents the projection of the angular momentum along the symmetry axis. . . . . 58
- 3.3 Angular momentum Coupling scheme for the deformed nuclei in the Strong(deformation aligned) and Weak (rotational alignment) coupling limits.  $K$  represents the projection of total angular momentum on the symmetry axis. . . . . 59
- 3.4 Pictorial representation of rotating deformed nucleus. Here,  $x_1, x_2, x_3$  represent the body fixed axes, and  $x, y, z$  represent the lab fixed axes. . . . 60

- 3.5 The effect of deformed nuclear potential and rotation on  $g_{9/2}$  orbital.  $N$ ,  $l$ , and  $j$  are the total oscillator quantum number, orbital angular momentum, and angular momentum, respectively. In the case of deformed nuclei,  $n_x$ ,  $\Lambda$  and  $\Omega$  are the components of  $N$ ,  $l$ , and  $j$ , along the symmetry axis.  $\pi$  and  $\alpha$  are the parity and signature quantum numbers in the case of rotating deformed nuclei. . . . . 61
- 4.1 Partial level scheme of  $^{125}\text{Xe}$ , which is mostly based on earlier works by A. Al-Khatib *et al.* and C.-B. Moon *et al.* . The transitions shown with "\*" are taken from as these transitions were very weak in our data. Only one new  $\gamma$  transition is shown with "#". To avoid contamination, the centroid of each transition was determined by gating on the nearest neighbor  $\gamma$  ray. The intensities of transitions in band 1 have been measured in the gate on the 486.3-keV  $\gamma$  ray while normalizing with respect to the intensity of the 644.5-keV one. Similarly, the intensities of transitions in bands 2, 3, and 4 were determined by gating on respective decay-out transitions. The width of each transition represents the normalized intensity of the corresponding transitions. Measurement of normalized intensity was not possible for the transitions with "\*" and energies 426.5, 583.1, and 573.7 keV, and hence the said transitions are shown in the level scheme by arrows having a width of 1.0. For more details, see table 4.1 . . . . . 73

- 4.2 Variation of the theoretical  $R_{DCO}$  value (black line) as a function of the mixing ratio  $\delta$  plotted for different  $\Delta I = 1$  transitions. The red lines correspond to the experimental value of  $R_{DCO}$  for the 590.8 (panel (a))- and 725.5 (panel (b))-keV transitions decaying from band 3 to band 1. The blue lines correspond to the experimental value of  $R_{DCO}$  for the 784.1 (panel (a))- and 944.0 (panel (b))-keV transitions decaying from band 2 to band 1. . . . . 78
- 4.3 The panels (a) and (b) represent the angular distribution plots for the 774.3-keV  $\gamma$  ray (quadrupole transition) and the 784.1-keV  $\gamma$  ray (dipole transition) determined with a coincidence gate on 486.3-keV (quadrupole transition)  $\gamma$  ray. Panels (c) and (d) represent the  $a_2 - a_4$  contour plots for the 774.3- and 784.1-keV transitions, respectively. The inset provides the  $\chi^2$  analysis for the experimental angular distribution of the corresponding transitions. . . . . 80
- 4.4 The upper panels (a), (b), and (c) represent the angular distributions for the 590.8-, 725.5-, and 839.8-keV ( $\Delta I = 1$ ) transitions with a coincidence gate placed on the 486.3-keV  $\gamma$  ray. The  $a_2 - a_4$  contour plots of the 590.8-, 725.5-, and 839.8-keV transitions are shown in the lower panels (d), (e), and (f). The corresponding  $\chi^2$  minimization is displayed in the insets. . . 81
- 4.5  $E2$  fraction with respect to spin for  $\Delta I = 1$   $\gamma$ -ray transitions between  $n_\omega = 1$  and  $n_\omega = 0$  wobbling bands in different nuclei in the low spin regime. . . 82
- 4.6 The panels (a) and (b) represent the angular distribution and  $a_2 - a_4$  contour plot for the 619.3-keV transition with a coincidence gate on the 486.3-keV  $\gamma$  ray. . . . . 83
- 4.7 Experimentally observed  $E_{wobb}$  energies with respect to spin for  $^{133}\text{La}$ ,  $^{127}\text{Xe}$ ,  $^{133}\text{Ba}$ ,  $^{135}\text{Pr}$ ,  $^{125}\text{Xe}$  [this work and TPSM result . . . . . 84

4.8	Excitation energies as a function of spin of bands 1, 2, 3, and 4 in $^{125}\text{Xe}$ . . . . .	85
5.1	Polarization sensitivity of the clover detector placed at the $90^\circ$ of the INGA array in the present experiment. . . . .	91
5.2	Partial level scheme of $^{114}\text{Te}$ based on present work and previous work . The newly observed transitions in the present work are shown in red color. The level energies for each level are represented by magenta color. The transitions marked by blue color are the ones that are already observed in previous work, but the placement of these transitions is modified in the present work. . . . .	92
5.3	Prompt $\gamma$ -rays observed in coincidence with 708.7-keV transition. The newly observed transitions are indicated by an asterisk in red color. . . . .	98
5.4	The panels (a) and (b) represent the variation of linear polarization ( $P$ ) as a function of $R_{DCO}$ at different values of $\delta$ for 125.9- and 895.9-keV transitions. The inset provides the $\chi^2$ analysis for the corresponding transitions. . . . .	98
5.5	The $\gamma$ - $\gamma$ coincidence spectra obtained from the gate on 936.2-keV dipole transition. The gamma transition with energy 529.0 keV and highlighted with symbol # belongs to $^{114}\text{Te}$ . However, the placement is doubtful. . . . .	99
5.6	Prompt $\gamma$ - $\gamma$ coincidence spectra gated by 871.2-keV transition. The 384.2-, 516.5-, 834.2-, and 843.2-keV newly observed transitions are $E1$ in nature. The placement of 405.9 keV gamma transition represented by # symbol could not be resolved in the present work. . . . .	100

- 5.7 The  $\gamma$ - $\gamma$  coincidence spectra obtained from the gate on 729.2-(a), and 790.2-keV (b) quadrupole transitions showing two newly observed interconnected transitions between bands b4 and b2. It is to be noted that the 596.4 keV gamma is different from 596.1. The 600.4 keV transition is a likely contamination from  $^{114}\text{Sb}$ . . . . . 101
- 5.8 The variation of linear polarization as a function of  $R_{DCO}$  at different values of  $\delta$  for 504.7 keV transition. The inset shows the  $\chi^2$  vs  $\tan^{-1} \delta$  plot giving the mixing ratio  $\delta = -0.09_{-10}^{+14}$ . . . . . 101
- 5.9 Prompt  $\gamma$ - $\gamma$  coincidence spectra with gate on 618.1-keV transition. . . . . 102
- 5.10 The variation of  $R_{DCO}$  with the mixing ratio ( $\delta$ ) of different multipoles ( $L$ ) for 815.4-keV transition. . . . . 102
- 5.11 The variation of linear polarization ( $P$ ) as a function of  $R_{DCO}$  at different values of mixing ratio ( $\delta$ ) for 815.4-keV transition. The inset shows the  $\chi^2$  vs  $\tan^{-1} \delta$  plot giving the mixing ratio  $\delta = -1.3_{-7}^{+10}$ . . . . . 103
- 5.12 Prompt  $\gamma$ - $\gamma$  coincidence spectra with gate on 655.3 keV transition. The transition labeled in blue color was observed to decay at a level energy of 1391.4 keV. In the present work, this transition is observed to decay to the level of 2450.0 keV. . . . . 104
- 5.13 Prompt  $\gamma$ - $\gamma$  coincidence spectra obtained from the gate on 635.5-(a) and 901.2-keV (b) transitions. . . . . 104
- 5.14 Prompt  $\gamma$ - $\gamma$  coincidence spectra obtained from the gate on 1123.1-keV transitions. . . . . 105
- 5.15 The variation of linear polarization ( $P$ ) as a function of  $R_{DCO}$  at different values of mixing ratio ( $\delta$ ) for 1034.7-keV transition. . . . . 105

5.16	Prompt $\gamma$ - $\gamma$ coincidence spectra obtained from the gate on 1034.7-keV transition. The 636.0 keV transition could not be placed because of unsatisfactory coincidence. The placement of 556.1- and 636-keV gamma transitions represented by # symbol could not be resolved in the present work. . . . .	106
5.17	The rotational frequency ratio between the negative and positive parity bands as a function of spin for nuclei in different mass regions. . . . .	106
5.18	Experimental $B(E1)/B(E2)$ ratios with respect to spin have been plotted for different nuclei. . . . .	107
5.19	The potential energy surface of $^{114}\text{Te}$ calculated using CDFT in 3D lattice space. The energies are normalized to the ground state with $(\beta_{20}, \beta_{30}) = (0.189, 0)$ . The contour interval is 0.2 MeV. . . . .	109
5.20	Comparison between experimental and calculated energy levels for $^{114}\text{Te}$ . . . . .	111
5.21	Potential energy surface plot from the ULTIMATE CRANKER for $^{114}\text{Te}$ at $I = 16_1^+ \hbar$ . . . . .	113
5.22	Potential energy surface plot for $^{114}\text{Te}$ at $I = 14_2^- \hbar$ . . . . .	114
5.23	Potential energy surface plot from the ULTIMATE CRANKER for $^{114}\text{Te}$ at $I = 7\hbar$ . The calculation predicts three minimum which are indicated by I, II, and III. . . . .	116
6.1	The asymmetry correction factor $a(E_\gamma)$ at different $\gamma$ -ray energies. The solid line corresponds to a linear fit of the data. . . . .	121
6.2	polarization sensitivity of the clover detector placed at the $90^\circ$ of the INGA array in the present experiment. . . . .	122
6.3	Partial level scheme of $^{119}\text{I}$ based on present work and previous work. . . . .	123

- 6.4 The  $\gamma$ - $\gamma$  coincidence spectrum observed from the different gates to represent the newly observed transitions. An asterisk symbol shows the newly observed transitions. . . . . 129
- 6.5 Figure shows the observation of 596.0-keV transition in the gate of 520.7-keV. . . . . 130
- 6.6 The panels (a) and (b) represent the angular distribution plots for the 833.5- and 843.9-keV transitions, respectively, in the gate of 337.0 keV ground state transition. The panels (c) and (d) represent the  $a_2 - a_4$  plots for the 833.5- and 843.9-keV transitions, respectively. The experimental values are shown in red, which were obtained in the gate of 337.0 keV (ground state transition). The inset provides the  $\chi^2$  analysis for the experimental angular distribution of the corresponding transitions. . . . . 131
- 6.7 The panels (a), (b), and (c) represent the perpendicular and parallel spectrum for polarization. The corresponding gates are mentioned in the footnote of Table 6.2. The panels (d), (e), and (f) represent the  $R_{DCO} - P$  contour plots for the 833.5-, 851.8-, and 843.9-keV transitions. The inset provides the  $\chi^2$  analysis for the experimental  $R_{DCO}$  vs.  $P$  of the corresponding transitions. . . . . 132
- 6.8 Comparison of  $\delta$  values obtained from the angular distribution method and  $R_{DCO}$  vs. polarization method. . . . . 133
- 6.9 The panels (a) and (b) represent the angular distribution plot for 366.6- and 386.1-keV transitions in the gate of 499.3 and 461.7 keV transitions, respectively. The panels (c) and (d) represent the  $a_2 - a_4$  contour plots of corresponding transitions. The inset provides the  $\chi^2$  analysis for the experimental angular distribution of the corresponding transitions. . . . . 134

- 
- 6.10 The panels (a), (b) and (c) represent the  $R_{DCO} - P$  contour plots for the 366.6-, 738.2 and 386.1 -keV transitions, respectively. The inset provides the  $\chi^2$  analysis for the experimental  $R_{DCO}$  vs.  $P$  values of the corresponding transitions. . . . . 135
- 6.11 Excitation energies as a function of spin of bands 1, 2, 3, and 4 in  $^{119}\text{I}$ . . . 136
- 6.12 Experimentally observed  $E_{wobb}$  energies with respect to spin for  $^{119}\text{I}$ ,  $^{136}\text{Nd}$ ,  $^{133}\text{Ba}$ ,  $^{151}\text{Eu}$  and  $^{129}\text{Cs}$ . . . . . 137
- 6.13 Figures (a), (b), (c), and (d) represent the experimental values of excitation energies, staggering parameter, energy difference, and transition probability ratios with respect to spin, respectively between bands 6 and 7. 138

# List of Tables

4.1	List of initial level energies ( $E_i$ ), $\gamma$ -rays energies ( $E_\gamma$ ), spins of initial levels ( $I_i$ ) and final levels ( $I_f$ ), and relative intensity of the $\gamma$ -transitions ( $I_\gamma$ ) in $^{125}\text{Xe}$ . . . . .	76
4.2	List of the energies of the $\gamma$ transitions, spins, experimental $a_2$ - $a_4$ values, $R_{DCO}$ values, mixing ratios ( $\delta_{E2/M1}$ ), $E2$ fractions ( $= \frac{\delta^2}{1+\delta^2}$ ) and transition probability ratios for corresponding $\Delta I = 2$ intra- and $\Delta I = 1$ inter-band $\gamma$ -ray transitions of $^{125}\text{Xe}$ . . . . .	82
5.1	The known $E2$ transitions of $^{114}\text{Te}$ and $^{112}\text{Sn}$ nuclei, produced in the present experiment, for which the value of $Q(E_\gamma)$ was measured. These values of $Q(E_\gamma)$ are used to obtain the coefficients a and b as shown in Fig. 5.1. . . . .	90
5.2	List of initial states ( $E_i$ ) and energies of $\gamma$ rays ( $E_\gamma$ ), spins, relative intensity ( $I_\gamma$ ), $R_{DCO}$ values, linear polarization asymmetry ( $\Delta_{asym}$ ), multipole mixing ratio ( $\delta_{E2/M1}$ ), and multipolarity ( $E\lambda/M\lambda$ ) of the $\gamma$ transition in $^{114}\text{Te}$ . . .	93
5.3	Measured $B(E1)/B(E2)$ ratios and deduced electric dipole moment in $^{114}\text{Te}$ .	108
5.4	Comparison of $B(E2)$ values for the band b1 obtained from the experiment and shell model calculations. . . . .	112
5.5	$B(E2)$ transition strength for the observed transition in $^{114}\text{Te}$ . . . . .	115

---

6.1	The known $E2$ transitions of $^{119}\text{I}$ , produced in the present experiment, for which the value of $Q(E_\gamma)$ was measured. These values of $Q(E_\gamma)$ are used to obtain the coefficients a and b as shown in Fig. 6.2. . . . . .	122
6.2	List of initial states ( $E_i$ ) and energies of $\gamma$ rays ( $E_\gamma$ ), spins, relative intensity ( $I_\gamma$ ), $R_{DCO}$ values, linear polarization asymmetry ( $\Delta_{asym}$ ), multipole mixing ratio ( $\delta_{E2/M1}$ ), and multipolarity ( $E\lambda/M\lambda$ ) of the $\gamma$ transition in $^{119}\text{I}$ . . . . .	124
6.3	Measured $B(E2)_{out}/B(E2)_{in}$ and $B(M1)_{out}/B(E2)_{in}$ values of interconnecting transitions from band 2 to 1 and 3 to 2 in $^{119}\text{I}$ . . . . .	136